Underwater Salp-Inspired Soft Body Contraction with Twisted Coiled Actuators

Ali Jones[1] and Joseph R. Davidson[1]

***Abstract*— Underwater compliant-body jet propulsion is among the most efficient of all animal locomotion. Multi-jet propulsion, a less common method of transit used by the Salp, offers a lower cost of transit, higher maneuverability, and redundancy in case of individual failure. Single-jetting robots have been created that are capable of tethered, repeatable swimming and steering. However, these designs were primarily inspired by squid, jellyfish, or other single-jet propulsors. In this work, we instead start with an individual module inspired by a salp chain. We analyze the shape change of different soft bodies activated by artificial muscles. By comparing the effect of body morphology and muscle activation sequence on volumetric change and extrapolated thrust, we can compare our results to those seen by salps. We achieve a maximum volumetric decrease during contraction of 26%.**

I. Introduction

Pulsed jet propulsion is one of the most efficient types of locomotion in the animal kingdom and is used by a variety of marine organisms from cephalopods to cnidaria [1]. In recent years, many underwater robots have been developed taking inspiration from squid, cuttlefish, jellyfish, and other single-jet propulsors [2]. This type of propulsion relies on the shape change of a compliant body to intake and expel fluid, creating thrust. In addition to having a low cost of transit and energy consumption, these soft-bodied propulsors create less disturbance to their environment than traditional rigid propeller-based designs [3].

In comparison, multi-jet propulsion is less common in both nature and robotics research despite a lower cost of transit, increased maneuverability, and redundancy [4]. One organism that locomotes with effective and efficient multi-jet propulsion is the salp. Salps are barrel-shaped pelagic tunicates that live in long chains of connected individuals, each capable of pulsed-jet propulsion. Salp chains are able to achieve asynchonous propulsion - in which different propulsors activate at varying times - allowing them to reduce drag forces from acceleration [5]. Additionally, salp chains are low-impact, highly compliant, and able to continue functioning if an individual unit fails.

Effective multi-jet propulsion relies on effective individual propulsive units. In the case of the salp, each individual moves by ingesting water through an anterior siphon and ejecting water through a posterior siphon via the contraction of discrete muscle bands arranged circumferentially around the tubular body (see Fig. 1, *top*). The individual salp is a unique and highly efficient jet propulsor for several reasons: their distinct intake and ejection valves avoid the need to reverse the ingested fluid direction; the valves are relatively large and the muscle bands contract slowly, leading to lower chamber pressures and jet velocities; their valve and muscle band configuration allows for a variety of whole-body motions, including accelerating, stopping, or swimming backward [6] [7].

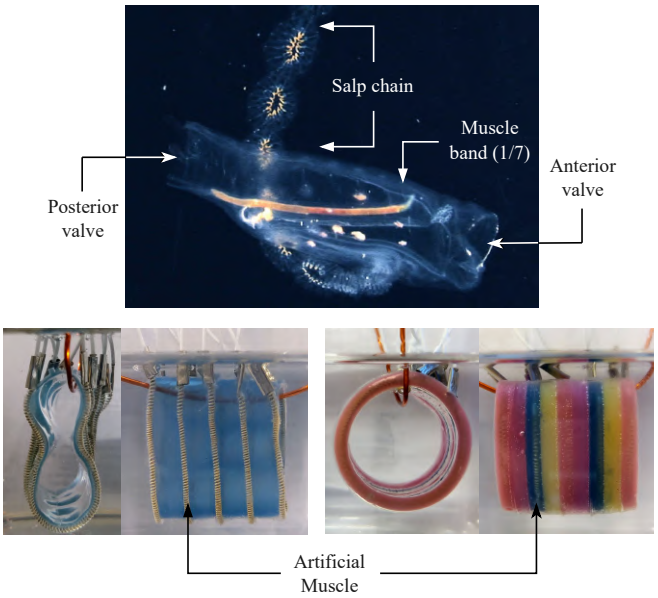

Fig. 1: (Top) An individual salp, Cyclosalpa affinis, in the foreground with a chain of salps in the background (Photo courtesy of Dr. Kelly Sutherland/University of Oregon). (Bottom) The two 3D body morphologies compared: a thin shell (*left*) and a cylindrical tube (*right*).

Inspired by the salp, we propose a compliant jet propulsive module powered by artificial muscles. In this work, we create multiple silicone bodies to study salp-based single-jet propulsion, focusing on the effects of body morphology and actuation sequences on shape change. To achieve this, we first manufactured artificial muscles and characterized their force and strain response to varying power inputs. We then embedded these artificial muscles into three different cylindrical soft bodies – one 2D, and two 3D – and analyzed their shape change. We used the measured shape change to calculate predicted thrust for the 3D bodies. *The specific contributions of this work are as follows*:

- We analyze the effects of body morphology, including wall thickness and muscle stacking, on contraction.

This work was supported in part by ONR grant number N00014-23-1-2171.

[1]Collaborative Robotics and Intelligent Systems (CoRIS) Institute, Oregon State University, Corvallis OR 97331, USA [jonesal9, joseph.davidson]@oregonstate.edu

- We compare sequenced, wave-like muscle contraction to simultaneous, whole-body contraction on whole-body volumetric change and thrust.

II. Related Work

A. Soft Jet Propulsors

Several soft underwater jet propulsors capable of repeatable motion have been developed that take inspiration from nature. The majority of these works are based on cephalopods and jellyfish and take advantage of the elastic restoring force of a compliant body to refill after contraction. We limit the scope of our background to vehicles that can swim freely or with an electrical tether and can achieve repeatable shape change.

Christianson et al. [8] created a cephalopod-inspired robot driven by a slip-gear mechanism that achieved a maximum thrust of 0.19N and speed of 32cm/s. Work by Bujard et al. [9] exploited material resonance with a piston-lever to greatly lower its cost of transit. Other works use cables as the primary actuation method. Serchi et al. [10] developed a silicone body driven by the cyclic actuation of cables with a crank mechanism to achieve a speed of 20cm/s, and Yang et al. [11] demonstrated origami-based shape change with the magic ball pattern that could move at 6.7cm/s.

Works based on jellyfish primarily consist of a semi-rigid body connected to a flexible flapping bell. Flapping jellyfish of this type driven by artificial muscles – shape memory alloys [12] and twisted coiled polymer actuators [13] – have reached speeds of 1.5mm/s, but required 600W of power. Varying from this design, Ye et al. [14] developed a fully-soft jellyfish actuated with liquid metal that reached a speed of 6mm/s at 7.5V.

Only a few works have created jet propulsors with distinct intake and ejection valves. The first is a salp-based, SMA powered silicone body with an active anterior valve and a posterior valve that could be angled (but not closed) to allow rotation. This design was able to reach speeds of 8mm/s at 5V [15]. The second is inspired by the scallop, with distinct valves and a silicone baffle to control the flow of water [16].

B. Artificial Muscles

In recent years, numerous artificial muscles have been developed to emulate desirable characteristics of biological muscles, including high efficiencies, high stresses and strains, and low specific power [17]. This work focuses on twisted-and-coiled polymer actuators (TCAs), artificial muscles made of highly twisted polymer thread, due to their large strains (40%), limited hysteresis, and ease of actuation [18]. Yip and Niemeyer [19] show that feedforward and feedback control can be used to predict TCA force and displacement in response to electrical power.

TCAs are manufactured by first twisting and then coiling polymer thread, amplifying the material properties of the polymer and creating an actuator that contracts linearly when heated [20]. By using a conductive polymer thread, most commonly silver coated nylon, Joule heating can be used for actuation. Two main types of TCAs exist: self-coiled, which allows coils to naturally form after the thread is twisted past coil nucleation; and mandrel-coiled, which are created by coiling twisted thread around a mandrel and heat-treating to retain the shape [20].

Both self-coiled and mandrel-coiled TCAs have been embedded in soft bodies to achieve motion. Sun et al. [21] created mandrel-coiled TCAs with reversible, repeatable strokes that return to their resting length without preload. These were embedded in silicone to create a soft gripper capable of 3D bending and torsion [22] and an underwater shape-morphing link [23]. Almubarak and Tadesse [24] embedded self-coiled TCAs in silicone skins to analyse the shape change created by different configurations and power inputs. TCAs have also been used to create crawling robots, including an inchworm [25] and lightweight tensegrity robot [26].

III. Methods

Here we describe the process for fabricating and analyzing the soft silicone modules. We begin with a brief description of relevant salp biology (III-A). We then present TCA fabrication and the characterization process (III-B). After embedding the TCAs in silicone structures (III-D) and immersing them in non-conductive mineral oil, we use image processing functions from OpenCV to estimate volume change for three different types of actuation sequences (III-E). From the volumetric flow rate, we use simple fluid mechanics to predict the bodies' generated thrust (III-F).

A. Salp-Inspired Design Parameters

While exact characteristics and morphologies vary depending on the species, most salps are smooth, transparent cylinders encircled by a number of muscle bands [7]. One full propulsion cycle can be broken into two parts. First, the anterior valve closes as the body muscle bands begin to contract. Water is expelled through the open posterior valve. Second, the muscle bands relax and the chamber pressure lowers, closing the posterior valve. The anterior valve opens as the elasticity of the body causes expansion, drawing in water from the front. *In this study, we focus on muscle and body contraction, leaving valve design and integration for future work.*

Early works identify key features of salp propulsion [6] [7]. Some of these features are tabulated below:

- Pulse rate: 0.5 - 2.5 Hz
- Speed: 3.3-6 cm/s
- Static thrust estimate per pulse: 0.6 - 2.3 mN
- Volume ejected in pulse: 30-50%
- Cost of transit: 0.6-2.1 $Jkg^{-1}m^{-1}$
- Chamber pressure: 80 - 128 Pa
- Body length: 3-12 cm

B. Twisted-Coiled Actuator Fabrication

The fabrication process for TCAs used in this work is adapted from the mandrel-coiled method [20] and work by Sun et al., 2021 [21]. In this process, twisted thread is coiled around a helical mandrel and heat-treated to achieve a desired shape.

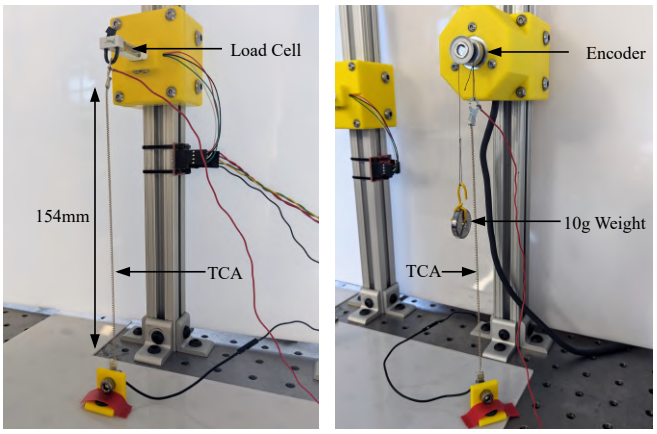

Fig. 2: Force (left) and strain (right) characterization setup.

1) **Create the helical mandrel**. A 24 gauge copper wire is wrapped around an 0.8mm⌀ carbon fiber rod using a custom machine. Two stepper motors rotate the rod while a lead screw moves a 3D printed traveler along its length. Copper wire is fed through the traveler, creating a uniform helical coil around the carbon fiber. The speed of the stepper motors are set to achieve a pitch angle of 22.5° between the coils, shown to achieve a large TCA stroke [21].
2) **Twist**. Silver-coated nylon 6,6 sewing thread (Shieldex 236 4-ply) is hung from a stepper motor with a 200g weight on the end. 700 revolutions per meter are applied to the thread without allowing the weight to rotate.
3) **Coil**. The twisted thread is coiled around the helical mandrel without losing tension or snarling. The ends are clipped to prevent untwisting and uncoiling.
4) **Anneal**. The coiled mandrel is heat-treated in an oven at 180°C for 2.5 hours.
5) **Pretrain**. To remove stresses brought about by the annealing process, the TCAs are activated to their maximum displacement with 3W of power several times.

C. TCA Experimental Setup

We used a testbed to characterize the force and strain response of TCAs to different power inputs. As shown in Fig. 2, the testbed included a 100g-rated load cell and quadrature encoder with sub-μm precision. TCAs attached to the load cell were pretensioned to 1g, and TCAs connected to the encoder via a pulley were prestrained with a 10g weight. We recorded force and strain for three different TCAs, each with a resistance of approximately 13.3Ω, at power increments of 1W - 4W. Higher power caused TCA degradation and breakage.

D. Embedding TCAs in a Soft Body

To explore the behavior of soft-body contraction, we embedded TCAs in silicone (Ecoflex-0030). We developed and compared the behavior of three different morphologies as shown in Fig. 4: a cylindrical cross section, tube, and thin shell.

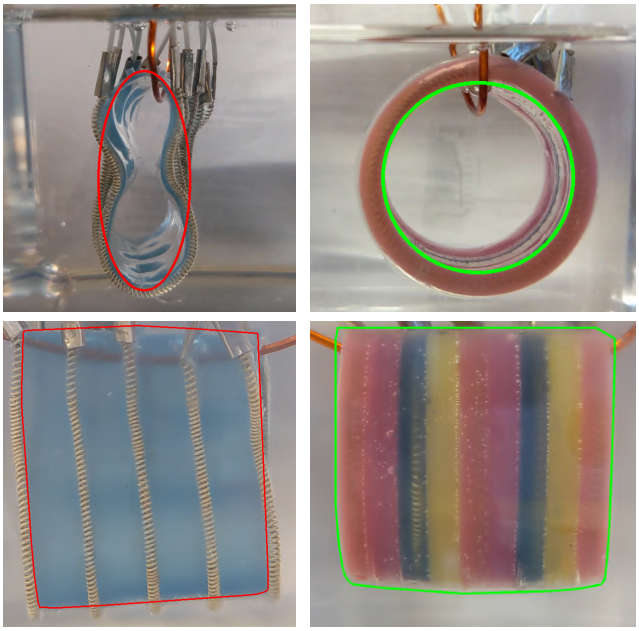

Fig. 3: Soft bodies with geometric primitives overlaid on the end (top row) and side (bottom row) areas. Shape change was more clearly seen from the side, so we used side contours as our primary area measurement and end contours to calculate volume and volumetric flow estimates.

1) Cross Section: We poured silicone in a 4mm deep, 32mm⌀ cylindrical mold with negative space forming a hollow ring through the midplane. We then threaded a TCA through this hollow ring, forming a 2D pulser (Fig. 4a).

2) Tube: To create a 3D body, we stacked five cross sections each separated by a blank – a cross section without negative space or a TCA. To ensure the body was as homogeneous as possible, we stacked the previously-cured layers on top of each newly poured layer, allowing the silicone to cure together. This created a 34mm long tube with 3mm thick walls and five muscle bands (Fig. 4b).

3) Shell: The second 3D body we created was only 1mm thick – 1/3 as thick as the cross section and shell – so we were unable to stack 2D sections. Instead, we poured a thin sheet and fixed it into a cylinder with SIL-poxy. We then wrapped five TCAs around this shell (Fig. 4c).

After we manufactured each body, we trimmed the TCAs to similar resistances and connected them to conductors with single barrel crimp sleeves. The tube and shell were then suspended in a clear tank of non-conductive mineral oil to emulate contraction underwater, while the cross section was laid flat on a thin film of mineral oil to eliminate friction.

E. Soft Body Contraction

To accurately measure the continuous shape-change of the soft bodies, we used a computer vision pipeline on videos of each contraction cycle. The cross section was viewed top-down (see the insets in Fig. 7), while the 3D bodies were tracked from the side and ends (Fig. 3). From these contours, we were able to track the body area over time and extrapolate

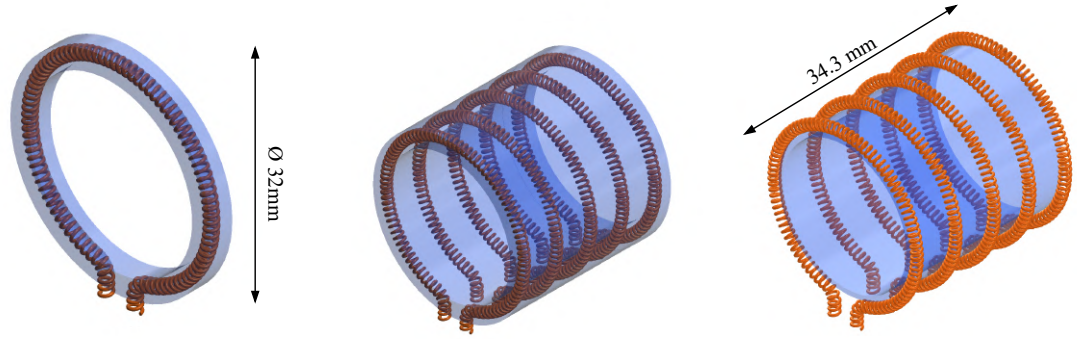

(a) Cross Section (b) Tube (c) Shell

Fig. 4: The three soft body morphologies compared in this study with dimensions. TCAs are encased in the silicone of the cross section (a) and tube (b) but are wrapped around the outer diameter of the shell (c).

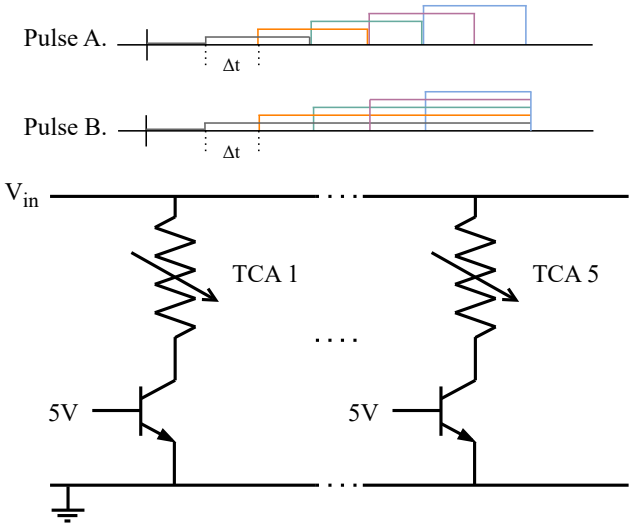

Fig. 5: The two sequenced pulses applied to the soft bodies (top) and the wiring schematic used for multi-tca activation (bottom). The magnitude applied to each TCA is the same, differences in height are for illustrative purposes only.

an estimate of jet thrust over the contraction cycle - assuming the front of the body was closed.

We activated the cross section with a single 5W pulse. For a more robust analysis of shape change, we used three different input sequences for the 3D bodies, shown in more detail in Fig. 8. To achieve controlled soft body contraction, we set up an array of transistors as diagrammed in Fig. 5 and used a microcontroller to create the desired pulse sequence.

F. Thrust Approximation

To estimate thrust generation, we extrapolate computer vision area measurements. Thrust (F_T) is a function of mass flow rate ($\dot{m}$) and outflow jet velocity (q) [27].

$$F_T = \dot{m}q \tag{1}$$

However, neither mass flow rate nor jet velocity are simple to calculate or measure. To eliminate these from equation (1), we rewrite mass flow rate in terms of an outflow friction coefficient (C_O), fluid density (ρ), outlet area (A_O), and outlet velocity.

$$\dot{m} = C_o \rho A_o q \tag{2}$$

$$\dot{m} = \rho \dot{V} \tag{3}$$

Combining 1 and 2 with 3, the relationship between mass flow rate and volumetric flow rate ($\dot{V}$), we arrive at an equation in terms of geometric parameters,

$$F_T = \frac{\rho \dot{V}^2}{C_o A_o} \tag{4}$$

where outlet area (A_O) and volumetric flow rate ($\dot{V}$) are estimated with image processing and numerical differentiation, respectively, fluid density (ρ) is known, and the outflow friction coefficient (C_O) is 0.6, an estimated value from salp thrust measurements [6].

IV. Results & Discussion

A. TCA Characterization

The TCA force and strain responses to different power levels are shown in Fig. 6. We achieved a maximum of $49.7 \pm 4.9\%$ strain and $425.3 \pm 13.7mN$ of force at a power of 4W, averaged over three different TCAs. We realized during characterization that ensuring all TCAs have similar initial resistances is critical to achieving similar responses. Upon contraction, TCA resistance decreases with length until all coils touch, at which point it increases. Differing initial resistances combined with this length-varying phenomenon causes a wider spread of responses.

In their 2017 work, Yip and Niemeyer showed that a self-coiled TCA has a first-order response to a step input in power [19]. We verified that this relationship holds for a mandrel-coiled TCA; first-order behavior can be seen in Fig. 6a and verified with function fitting. Therefore, we can identify time constants as the time required for the TCA to reach 63% of

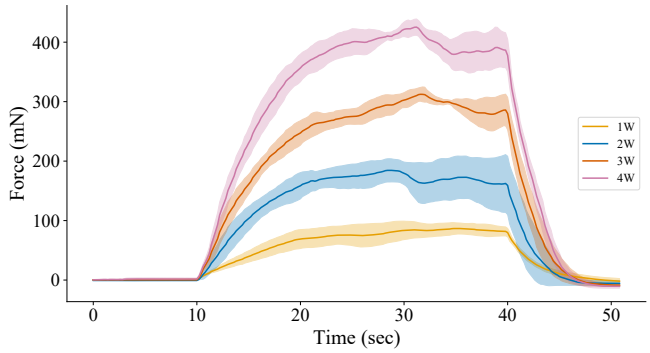

(a) Measured force in response to different power levels.

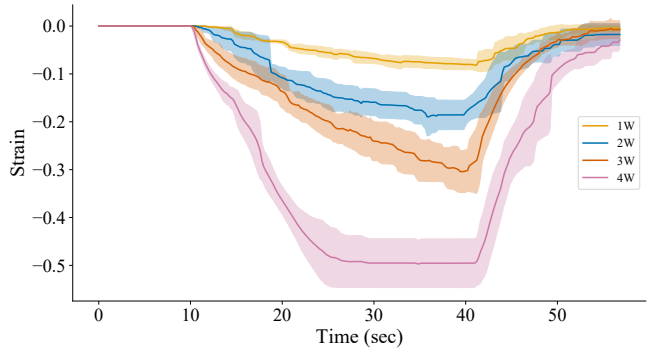

(b) Measured strain in response to different power levels.

Fig. 6: TCA characterization results. Each solid line shows the mean of three different TCAs with shaded regions for standard deviation.

TABLE I: Time constants for force response to power step input with $1g$ preload.

Input Type	Time Constant τ (sec)			
	1 Watt	*2 Watts*	*3 Watts*	*4 Watts*
Heating	6.6	5.4	6.2	6.0
Cooling	2.4	2.0	2.4	2.6

its steady state value. Time constants for heating and cooling cycles are reported in Table I.

We sized the soft bodies based on previously reported work by Sun et. al [21], which demonstrated TCAs that reached a displacement of 40mm in 1.5 seconds. In a cylinder with a 32mm diameter, this displacement would eject 45% of its volume per second - a value corresponding to those seen by salps. Our TCAs, however, took 8 seconds to reach this displacement.

B. Soft Body Response

The area change of the cross section to a 5W pulse can be seen in Fig. 7. The internal area took 25 seconds to change from $567.3 \pm 18.8 mm^2$ to $399.6 \pm 23.1 mm^2$. This is a $29.6 \pm 13.0\%$ change, a value within one standard deviation of the volume ejected by a salp per cycle but at a much slower rate.

For the 3D bodies, varying both morphology and activation sequence created a different shape change. Fig. 8 shows the

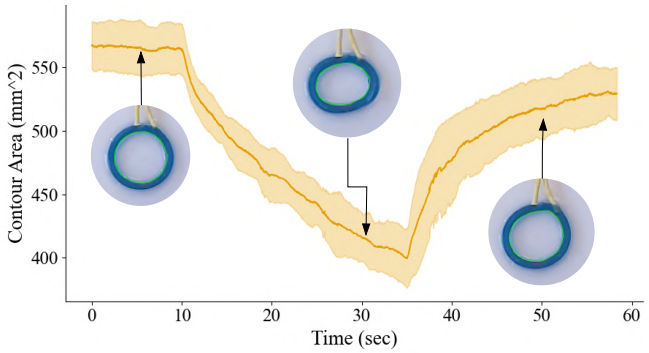

Fig. 7: Area change in response to a 5W step in power, averaged over two trials each for three different cross sections.

shape change of the shell and tube for the three sequences. The shell achieved greater overall contraction than the tube – 23.5% decrease in volume, compared to 7.42% – while the tube had a more consistent response.

1) **All TCAs activated simultaneously:** both the shell and tube saw immediate contraction and a larger magnitude slope than the other two sequences. The fast response caused this sequence to produce the largest peak in thrust in both soft bodies, but the TCAs in the tube had to work against the larger elastic mass, causing a lower overall thrust value than the shell. The shell was fully contracted after 30 seconds, while the tube required the full 60 second pulse.
2) **TCAs activated in sequence:** the shell and tube reached full contraction, but took longer than the first sequence. This is a more efficient sequence, as it applies incrementally increasing power that only reaches the level of (1) at the final activation. However, the thrust that would be generated by this sequence is much lower in both morphologies due to the slower volumetric change.
3) **TCAs activated and released:** the shell and tube began contracting as in (2) but weren't able to reach full contraction. Once the first TCAs began releasing, the bodies expand quicker than the remaining TCAs can contract. The thrust generated by this sequence is of a similar magnitude to (2).

Based on our TCA characterization, we would expect the maximum strain (50%, Fig. 6b) of an unhindered TCA to create a 75% decrease in volume. Instead, we see a 23.5% and a 7.42% decrease in the shell and tube volume, respectively. This is significantly less, indicating that the combined forces of the silicone elasticity and friction impede TCA performance.

The difference in the performances of the two 3D morphologies is primarily because the TCAs have to work against more material in the tube, including the inert blanks in between each stacked cross section. This added material also likely acts as an insulator, preventing the TCAs from shedding heat and limiting some of their contraction. Further analysis could investigate the impacts of temperature on

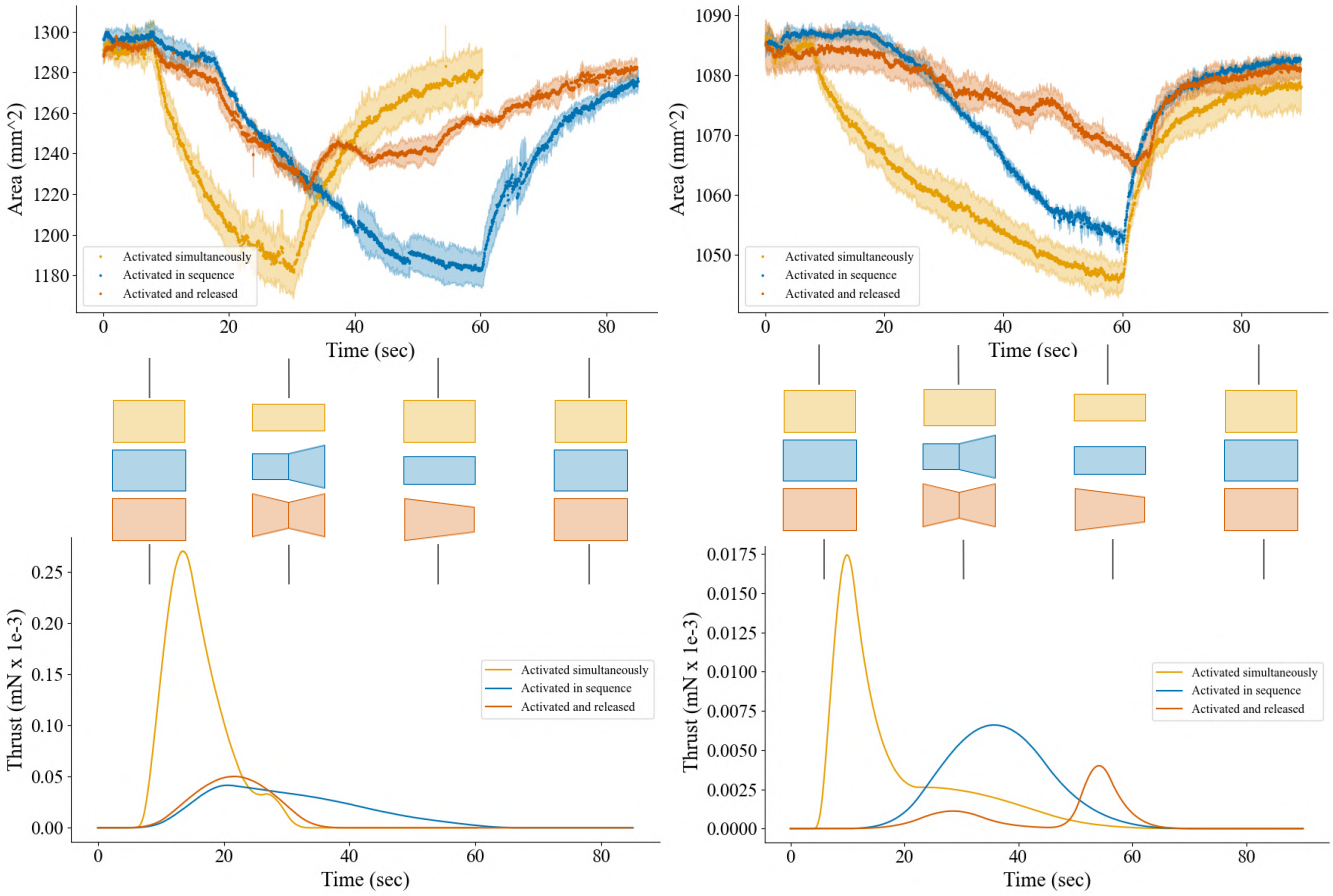

Fig. 8: Shell (left) and tube (right) side area response to different input pulses with extrapolated thrust estimates. The colored shapes are simplified representations of the soft body activated by the three different pulses. Yellow shows simultaneous activation of all five TCAs. Blue and red both show sequenced activation with a five second delay between TCAs. The blue sequence activates and holds each TCA, while the red sequence releases each TCA after 10 seconds.

volumetric change.

The maximum estimate of thrust generated by the shape change was by the shell with all TCAs activated at once. Thrust peaked at 0.27e-3 mN, three orders of magnitude smaller than a salp. This is likely less than a salp for several reasons: the pulse rate of a salp is eight to 15 times greater than our soft bodies, increasing the volumetric flow rate; the cross sectional area of a salp is smaller; salp posterior valves are shaped to form spherical vortex rings of ejected water, a phenomenon shown to increase thrust. Creating faster actuators, longer and skinnier morphologies, and engineered valves could likely increase thrust of these soft bodies.

V. Conclusion

In this paper, we explore salp-inspired, compliant body shape change driven by twisted-and-coiled polymer actuators. We first characterize the force and strain generated by TCAs before embedding them in three different soft bodies. We achieved a maximum of 29.6% contraction in a 2D cylindrical cross section, which decreased to 7.41% when expanded to a full 3D cylinder. A shell of the same dimensions as the tube but with 1/3 the wall thickness reached a volumetric contraction of 23.5%. Additionally, we compared the shape change brought about by different input sequences. We saw that some sequences were able to achieve the same maximum contraction as whole-body simultaneous activation, while other wave-like pulses were unable to do so. Future work will include further investigation into different materials and morphologies, such as bistable mechanisms, to best utilize TCA activation. Furthermore, adding controlled anterior and posterior valves will allow us to verify thrust generation estimates and work toward a self-propulsive robot.

References

[1] J. H. Costello, S. P. Colin, J. O. Dabiri, B. J. Gemmell, K. N. Lucas, and K. R. Sutherland, "The hydrodynamics of jellyfish swimming," *Annual Review of Marine Science*, vol. 13, no. 1, pp. 375–396, Jan. 3, 2021.

[2] Q. Zhu and Q. Xiao, "Physics and applications of squid-inspired jetting," *Bioinspiration & Biomimetics*, vol. 17, no. 4, p. 041 001, Jul. 1, 2022.

[3] S. Cherangara Subramanian, T. Le, J. Olson, S. Bhat, and S. Redkar, "Design and development of an unmanned underwater vehicle (UUV) in the form of a cuttlefish," in *Volume 4B: Dynamics, Vibration, and Control*, Pittsburgh, Pennsylvania, USA: American Society of Mechanical Engineers, Nov. 9, 2018, V04BT06A020.

[4] K. T. Du Clos, B. J. Gemmell, S. P. Colin, J. H. Costello, J. O. Dabiri, and K. R. Sutherland, "Distributed propulsion enables fast and efficient swimming modes in physonect siphonophores," *Proceedings of the National Academy of Sciences*, vol. 119, no. 49, e2202494119, Dec. 6, 2022.

[5] K. R. Sutherland and D. Weihs, "Hydrodynamic advantages of swimming by salp chains," *Journal of The Royal Society Interface*, vol. 14, no. 133, p. 20 170 298, 2017.

[6] Q. Bone and E. R. Trueman, "Jet propulsion in salps (tunicata: Thaliacea)," *Journal of Zoology*, vol. 201, no. 4, pp. 481–506, Dec. 1983.

[7] L. P. Madin, "Aspects of jet propulsion in salps," *Canadian Journal of Zoology*, vol. 68, no. 4, pp. 765–777, Apr. 1, 1990.

[8] C. Christianson, Y. Cui, M. Ishida, *et al.*, "Cephalopod-inspired robot capable of cyclic jet propulsion through shape change," *Bioinspiration & Biomimetics*, vol. 16, no. 1, p. 016 014, Jan. 2020, Publisher: IOP Publishing.

[9] T. Bujard, F. Giorgio-Serchi, and G. D. Weymouth, "A resonant squid-inspired robot unlocks biological propulsive efficiency," *Science Robotics*, vol. 6, no. 50, eabd2971, Jan. 20, 2021.

[10] F. Giorgio-Serchi, A. Arienti, and C. Laschi, "Underwater soft-bodied pulsed-jet thrusters: Actuator modeling and performance profiling," *The International Journal of Robotics Research*, vol. 35, no. 11, pp. 1308–1329, Sep. 1, 2016, Publisher: SAGE Publications Ltd STM.

[11] Z. Yang, D. Chen, D. J. Levine, and C. Sung, "Origami-inspired robot that swims via jet propulsion," *IEEE Robotics and Automation Letters*, vol. 6, no. 4, pp. 7145–7152, Oct. 2021, Conference Name: IEEE Robotics and Automation Letters.

[12] P. Singh Matharu, Z. Wang, J. H. Costello, S. P. Colin, R. H. Baughman, and Y. T. Tadesse, "SoJel –a 3d printed jellyfish-like robot using soft materials for underwater applications," *Ocean Engineering*, vol. 279, p. 114 427, Jul. 2023.

[13] A. Hamidi, Y. Almubarak, Y. M. Rupawat, J. Warren, and Y. Tadesse, "Poly-saora robotic jellyfish: Swimming underwater by twisted and coiled polymer actuators," *Smart Materials and Structures*, vol. 29, no. 4, p. 045 039, Apr. 1, 2020.

[14] J. Ye, Y.-C. Yao, J.-Y. Gao, *et al.*, "LM-jelly: Liquid metal enabled biomimetic robotic jellyfish," *Soft Robotics*, soro.2021.0055, Apr. 29, 2022.

[15] S. Guo, S. Sun, and J. Guo, "Design of a sma-based salps-inspired underwater microrobot for a mother-son robotic system," in *2017 IEEE International Conference on Mechatronics and Automation (ICMA)*, Aug. 2017, pp. 1314–1319.

[16] Y. Wang, S. Pang, H. Jin, *et al.*, "Development of a biomimetic scallop robot capable of jet propulsion," *Bioinspiration & Biomimetics*, vol. 15, no. 3, p. 036 008, Mar. 20, 2020.

[17] J. Wang, D. Gao, and P. S. Lee, "Recent progress in artificial muscles for interactive soft robotics," *Advanced Materials*, vol. 33, no. 19, p. 2 003 088, May 2021.

[18] C. Lamuta, "Perspective on highly twisted artificial muscles," *Applied Physics Letters*, vol. 122, no. 4, p. 040 502, Jan. 23, 2023.

[19] M. C. Yip and G. Niemeyer, "On the control and properties of supercoiled polymer artificial muscles," *IEEE Transactions on Robotics*, vol. 33, no. 3, pp. 689–699, Jun. 2017, Conference Name: IEEE Transactions on Robotics.

[20] C. S. Haines, M. D. Lima, N. Li, *et al.*, "Artificial muscles from fishing line and sewing thread," *Science*, vol. 343, no. 6173, pp. 868–872, Feb. 21, 2014.

[21] J. Sun, B. Tighe, Y. Liu, and J. Zhao, "Twisted-and-coiled actuators with free strokes enable soft robots with programmable motions," *Soft Robotics*, vol. 8, no. 2, pp. 213–225, Apr. 1, 2021.

[22] J. Sun and J. Zhao, "Modeling and simulation of soft robots driven by embedded artificial muscles: An example using twisted-and-coiled actuators," in *2022 American Control Conference (ACC)*, Jun. 2022, pp. 2911–2916.

[23] J. Sun, B. Pawlowski, and J. Zhao, "Embedded and controllable shape morphing with twisted-and-coiled actuators," in *2018 IEEE/RSJ International Conference on Intelligent Robots and Systems (IROS)*, Oct. 2018, pp. 5912–5917.

[24] Y. Almubarak and Y. Tadesse, "Twisted and coiled polymer (TCP) muscles embedded in silicone elastomer for use in soft robot," *International Journal of Intelligent Robotics and Applications*, vol. 1, no. 3, pp. 352–368, Sep. 2017.

[25] C. Wu, Z. Zhang, and W. Zheng, "A twisted and coiled polymer artificial muscles driven soft crawling robot based on enhanced antagonistic configuration," *Machines*, vol. 10, no. 2, p. 142, Feb. 16, 2022.

[26] D. Zhou, Y. Liu, X. Tang, J. Sun, and J. Deng, "A lightweight and multimotion crawling tensegrity robot driven by twisted artificial muscles," *IEEE Transactions on Industrial Electronics*, vol. 69, no. 11, pp. 11 447–11 457, Nov. 2022.

[27] W. Johnson, P. D. Soden, and E. R. Trueman, "A study in jet propulsion: An analysis of the motion of the squid, *Loligo Vulgaris*," *Journal of Experimental Biology*, vol. 56, no. 1, pp. 155–165, Feb. 1, 1972.